Ab initio simulation of $(Ba,Sr)TiO_3$ and $(Ba,Ca)TiO_3$ perovskite solid solutions

Leonid L. Rusevich[a,*], Guntars Zvejnieks[a], Eugene A. Kotomin[a,b]

[a] Institute of Solid State Physics, University of Latvia, 8 Kengaraga str., Riga LV-1063, Latvia

[b] Max Planck Institute for Solid State Research, Heisenbergstr. 1, Stuttgart D-70569, Germany

Abstract. The results of *ab initio* (first-principles) computations of structural, elastic and piezoelectric properties of $Ba_{(1-x)}Sr_xTiO_3$ (BSTO) and $Ba_{(1-x)}Ca_xTiO_3$ (BCTO) perovskite solid solutions are presented, discussed and compared. Calculations are performed with the CRYSTAL14 computer code within the linear combination of atomic orbitals (LCAO) approximation, using advanced hybrid functionals of the density-functional-theory (DFT). Supercell model allows us to simulate solid solutions with different chemical compositions (x = 0, 0.125 and 0.25) within ferroelectric tetragonal phases (x<0.3) of both solid solutions. It is shown that configurational disorder has to be taken into account in simulations of BCTO solid solutions, while for BSTO this effect is rather small. Both BSTO and BCTO show significantly enhanced piezoelectric properties, in a comparison with pure $BaTiO_3$. However, these solid solutions demonstrate opposite behaviour of a tetragonal ratio c/a and elastic constants as the functions of chemical composition. It is predicted that due to decrease of the elastic constants in BCTO, it has much higher converse piezoelectric constants than BSTO.

Keywords: perovskite solid solution; lead-free piezoelectric; ab initio; first-principles computation; density functional theory (DFT).

[*] Corresponding author.
E-mail: leorus@inbox.lv (L.L. Rusevich)

1. Introduction

In 1839, in the Ural Mountains of Russia, new mineral $CaTiO_3$ was discovered by Gustav Rose and named *perovskite* after Russian mineralogist L.A. Perovski. Later this name was used for a designation of large class of compounds with the same (ABO_3) crystalline structure. ABO_3-type compounds are interesting for materials science because of their ferroelectric and piezoelectric properties. Perovskite-type ferroelectrics are important materials for many technological applications, this is why they have been intensively investigated for a long time [1–4]. So far, lead-zirconate-titanate (PZT) is the most widely used piezoelectric material. Nowadays interest is increased in developing of "green" piezoelectric materials due to the lead toxicity [5]. $BaTiO_3$ (BTO) is a typical ferroelectric material with a perovskite-type structure. Although piezoelectric properties and temperature stability of pure BTO are worse than PZT, the reasonable large piezoelectric response of BTO makes it a promising material for novel "green" BTO-based piezoelectric compounds [6,7].

Development of new lead-free materials with good piezoelectric properties is a challenging problem. Chemical modification is the common approach for tuning dielectric and electromechanical properties of ferroelectrics. In perovskites, doping generally involves the replacement of either A- or B-type cations. In this work, we consider change of functional properties of BTO upon the chemical substitution of Ba atoms (A cations) by isovalent Sr or Ca atoms, i.e., $Ba_{(1-x)}Sr_xTiO_3$ (BSTO) and $Ba_{(1-x)}Ca_xTiO_3$ (BCTO) solid solutions with a perovskite structure. We investigate these compounds by means of first-principles calculations, with a focus on structural, elastic and piezoelectric properties, ending with conclusions about similarities and differences in behaviour of these two systems.

From a structural point of view, the high-temperature phases of BTO, $SrTiO_3$ (STO) and $CaTiO_3$ (CTO) have the ideal cubic structure, where Ti ion sits in the center of a cube and are octahedrally coordinated to the 6 nearest O ions. Such structure has centrosymmetric *Pm-3m* space group (SG 221) symmetry and therefore cannot be piezoelectric and ferroelectric. However, the situation changes upon decreasing the temperature. In BTO, at 393 K (at ambient pressure), Ti ions are displaced from the cube center along one of main cube axes, which leads to a structural (from cubic to tetragonal *P4mm*, SG 99) and paraelectric-ferroelectric phase transition accompanied by spontaneous polarization directed parallel to the tetragonal edge of the unit cell. With the further cooling, BTO undergoes two more inter-ferroelectric structural transitions: at 278 K to the orthorhombic phase (*Amm2*, SG 38) and at 183 K to the rhombohedral phase (*R3m*, SG 160). In contrast to BTO, STO and CTO do not show

piezoelectric properties over whole temperature range. STO and CTO belong to a family of incipient ferroelectrics or quantum paraelectrics [8]. At around 105 K, STO undergoes a structural phase transition from the paraelectric cubic phase to another paraelectric tetragonal phase (*I4/mcm*, SG 140), i.e., it has a cubic structure at room temperature. CTO has not been studied in such detail as BTO and STO. On decreasing temperature, CTO undergoes a sequence of structural phase transitions, but the number of these transitions and exact phase transition temperatures are still the subject of debate ([9] and references therein). Thus, Yashima and Ali [9,10] reported two subsequent phase transitions through neutron powder diffraction measurements in the temperature range 296 K – 1720 K. These are structural transitions from the cubic phase to a tetragonal (*I4/mcm*, SG 140) at ~1635 K and from the tetragonal to an orthorhombic (*Pbnm*, SG 62) at ~1510 K.

The aim of this work is the theoretical study and comparison of structural and electromechanical properties of BSTO and BCTO solid solutions. For BTO and STO complete solubility occurs, and, thus, $Ba_{(1-x)}Sr_xTiO_3$ solid solution may be obtained for a whole range of dopant concentration ($x = 0 – 1$). In contrast, BTO and CTO are only partially miscible and form the $Ba_{(1-x)}Ca_xTiO_3$ solid solution only up to the solubility limit of Ca, $x \sim 0.25 – 0.30$ [11,12]. It is known from experiments that at room temperature and around $x \approx 0.3$ BSTO undergoes a ferroelectric-paraelectric and structural (from tetragonal to cubic) phase transition, i.e., for higher Sr concentrations this solid solution no longer exhibits piezoelectric properties [13,14]. The experiments, concerning BCTO solid solutions, confirm its existence in the tetragonal phase up to the limit of solubility (at least $x \sim 0.25$; this limit can vary depending on processing) [11,12,15]. Moreover, experiments show the possibility of using BCTO solid solutions as piezoelectrics with high piezoelectric performance [11,15]. Direct comparison of BSTO and BCTO solid solutions has been performed in a few experimental and theoretical works [12,16], but these studies have focused rather on local structures and structural properties than elastic and piezoelectric properties.

Thus, in this study we focus our attention on the properties of tetragonal (room temperature) phases of BSTO and BCTO perovskite solid solutions. Computer simulations of these solid solutions are based on an *ab initio* (first-principles) approach and were performed with use of supercell calculations. Obtained structural, elastic and piezoelectric properties for both solid solutions at different chemical compositions are compared below.

2. Computational details

Methods of calculations, used in this work, have previously been described in detail in our paper [17], devoted to BSTO simulation. Here only basic information and details specific to the present study are given.

We performed our computations within the approximation of linear combination of atomic orbitals (LCAO) of the density functional theory (DFT) by means of the computer code for quantum chemical *ab initio* simulations CRYSTAL14 [18]. Three hybrid exchange-correlation functionals were used during the computations: PBE0 functional (PBE exchange functional, combined with 25% of Hartree-Fock (HF) exchange and the PBE correlation functional), B1WC functional (Wu-Cohen WCGGA exchange functional with 16% of HF exchange and the Perdew-Wang PWGGA correlation functional) and B3LYP functional (a three parameter functional, which combines BECKE exchange functional with 20% of HF exchange and LYP (Lee-Yang-Parr) correlation functional with NONLOCAL parameters 0.9 and 0.81) [19]. Basis sets with Hay and Wadt small core effective core pseudopotential were used for Ba, Ti and Sr atoms [20], while the all-electron basis sets — for description of O [21] and Ca [22] atoms.

For calculations on BSTO and BCTO solid solutions we used a 2×2×2 supercell, based on the tetragonal (SG 99) BTO unit cell. This supercell contains 40 atoms (8 unit cells) and allowed us to study ordered $Ba_{(1-x)}Sr_xTiO_3$ and $Ba_{(1-x)}Ca_xTiO_3$ solid solutions with different chemical compositions (Sr/Ba and Ca/Ba ratio). We replaced one or two Ba atoms by Sr or Ca atoms and thus considered 3 different dopant concentrations: x=0 (without substitution; pure BTO), x=0.125 (replacement of one Ba atom by dopant atom) and x=0.25 (replacement of two Ba atoms by dopant atoms) — according to that fact, that BSTO and BCTO solid solutions reveal tetragonal symmetry with ferroelectric and piezoelectric properties at room temperature for $x \leq 0.25$–0.3. In order to preserve maximal symmetry and to accelerate the calculations, for the composition x=0.125 we replaced the Ba atom at the origin of coordinates. For the x=0.25 composition we also replaced one Ba atom at the origin as well as one other. In this case, for the 40-atom supercell, we have 7 different possibilities to choose a second atom. The effect of this configurational disorder (different arrangement of A atoms) was considered in detail in [17], where all 7 configurations in $Ba_{0.75}Sr_{0.25}TO_3$ solid solution were discussed. In brief, for the x=0.25 composition, the 7 different substitutions lead to 3 cases where the system symmetry remains tetragonal and 4 cases where the symmetry is reduced to orthorhombic. As was shown [17], the effect of configurational disorder for BSTO is small enough (less than 10% and 4% for piezoelectric and elastic properties, respectively, and much less for structural and electronic

parameters). However, our computations reveal that the effect of configurational disorder for BCTO is far larger (see below for details). Hence, it is necessary to consider this in the study of BCTO solid solution. Therefore, in this work we perform averaging of properties of both solid solutions (for their correct comparison) on three tetragonal configurations. Moreover, a high level of DFT integration accuracy ("extra extra large grid" XXLGRID [19]) was used for computations of BCTO properties (it was especially important for calculations of elastic and piezoelectric properties). Though the XLGRID parameter ensured stable results for BSTO solid solutions, the BSTO data were recalculated with the XXLGRID parameter to allow for correct direct comparison with the results from the BCTO solid solutions.

A few words should be said here about methods of computation of elastic and piezoelectric properties of crystals. Fully-automated procedures for calculating of elastic and piezoelectric constants are implemented in the CRYSTAL14 program. Elements of elastic and direct piezoelectric tensors are calculated based on fully-optimized and deformed geometries — elastic constants as the second derivatives of total energy with respect to pairs of lattice deformations, but direct piezoelectric constants via the Berry phase approach [19]. At the same time, simple relation exists between the direct and converse ($\mathbb{e}$ and $\mathbb{d}$) piezoelectric tensors and the elastic tensor $\mathbb{C}$: $\mathbb{d} = \mathbb{e}\ \mathbb{C}^{-1}$. Thus, tensor $\mathbb{d}$ is calculated based on $\mathbb{C}$ and $\mathbb{e}$ tensors, calculated earlier.

3. Results and discussion

In order to estimate the quality of calculations with our computational setup (first of all, chosen functionals and basis sets), before performing the solid solution computations, we calculated basic properties of pure BTO, STO and CTO and compared them with the experimental data. The lattice constants for cubic structures (SG 221) of BTO, STO and CTO crystals, calculated using three hybrid exchange-correlation functionals, as well as their experimental values, are given in Table 1. This table demonstrates that both theoretical and experimental lattice constants decrease with decreasing of A cation size (Ba, Sr or Ca) in the cubic phase of BTO, STO and CTO perovskites.

Table 1. Calculated and experimental lattice constants (Å) for cubic phases of BTO, STO and CTO.

	PBE0	B1WC	B3LYP	Expt.
BTO	3.993	3.975	4.037	3.996 [23]
STO	3.901	3.884	3.937	3.905 [24]
CTO	3.850	3.835	3.882	3.887 [10]

The PBE0 functional gives the best (and excellent) agreement with the experimental data for BTO and STO crystals, whereas the B3LYP functional shows the worst results. In contrast, for the CTO crystal the B3LYP functional gives the best agreement with experiment. However, it is necessary to notice here, that the cubic phase of CTO is a very high temperature phase (above ~1630 K) and, therefore, agreement between results of *ab initio* calculations and experiment may not be so remarkable.

The results of calculations of lattice constants, bulk modulus and band gap for the orthorhombic (*Pbnm*, SG 62) phase of CTO and the corresponding experimental data are given in Table 2. Note that the *Pbnm* crystal structure consists of 4 units of ideal cubic perovskite structure; therefore 20-atom unit cell is used in the calculations of the orthorhombic CTO phase.

Table 2. Calculated and experimental lattice constants (*a*, *b*, *c*), bulk modulus *B* and band gap E_g for the orthorhombic phase of CTO.

	PBE0	B1WC	B3LYP	Expt.
a (Å)	5.372	5.343	5.412	5.371 [10], 5.387 [25]
b (Å)	5.445	5.425	5.497	5.428 [10], 5.439 [25]
c (Å)	7.629	7.590	7.690	7.627 [10], 7.646 [25]
B (GPa)	196	199	185	171 [26], 177 [27]
E_g (eV)	4.56	3.77	4.07	3.4 [28]

The PBE0 and B1WC functionals exhibit the best results in calculations of lattice constants, whereas the B3LYP functional gives the best agreement with the experiment for bulk modulus, but B1WC functional is again (as well as in ref. [17]) the most suitable for the calculations of band gap. Calculations by means of all three functionals yield the direct band gap for orthorhombic phase of CTO, while for the cubic phase of CTO we obtain the indirect band gap in agreement with [29]. Note that Moreira *et al*. [25] obtained a direct band gap of 3.98 eV for the orthorhombic phase of CTO using the B3LYP functional in CRYSTAL06. It should be noticed, too, that experimental lattice constants in Table 2 are room temperature values. The temperature dependence of lattice constants for the orthorhombic and cubic phases of CTO is available in ref. [10] and for the orthorhombic phase (7 K – 400 K) in [30]. Information about the experimental CTO band gap, obtained by different methods and at different conditions, is presented in ref. [31]. Some experimental and calculated data for different ABO_3 perovskites may be found in ref. [32].

Let us start discussion of BSTO and BCTO solid solutions. We begin with a consideration of the structural parameters of these crystals (in the tetragonal phase) at different dopant concentrations. These data are presented in Table 3. However, before discussion, it is necessary

to return to the question of the configurational disorder. Data for x=0.25 composition (2 Ba atoms are replaced by dopant atoms) represent averaging on three tetragonal configurations (see below). It is not so important for BSTO, because the difference in contributions of each atomic configuration is small, but for BCTO it is necessary to take into account these differences. For example, in the simulation of the x=0.25 composition of BSTO, the tetragonal ratios c/a for 3 configurations are 1.029, 1.027, 1.028 (average — 1.028) for PBE0 functional; 1.014, 1.013, 1.014 (average — 1.014) for B1WC; and 1.067, 1.056, 1.058 (average — 1.060) for B3LYP. The maximal differences of total electronic energies (after geometry optimizations) between these three tetragonal configurations are 0.06 eV, 0.08 eV and 0.09 eV for the calculations by means of PBE0, B1WC and B3LYP functionals, respectively. At the same time, dispersion of the parameters for BCTO solid solutions is far larger: tetragonal ratios are 1.065, 1.038, 1.044 (average — 1.049) for the PBE0 functional; 1.033, 1.018, 1.025 (average — 1.025) for B1WC; 1.157, 1.101, 1.110 (average — 1.123) for B3LYP. The maximal differences of total electronic energies are 0.23 eV, 0.21 eV and 0.33 eV for PBE0, B1WC and B3LYP functionals, respectively. However, even such differences in the electronic energies are insufficient for a reliable conclusion about preference of any configuration. Such decision should be based on the analysis of the Gibbs free energies, but it lies beyond the scope of this work.

Table 3. The lattice constants (a=b and c) of BSTO and BCTO crystals at different chemical compositions x, calculated by three functionals.

	PBE0			B1WC			B3LYP		
x=	0	0.125	0.25	0	0.125	0.25	0	0.125	0.25
				BSTO					
a (Å)	3.971	3.963	3.955	3.962	3.954	3.945	3.991	3.982	3.976
c (Å)	4.131	4.100	4.066	4.050	4.026	4.000	4.292	4.262	4.215
				BCTO					
a (Å)	3.971	3.950	3.931	3.962	3.944	3.927	3.991	3.954	3.925
c (Å)	4.131	4.131	4.122	4.050	4.041	4.026	4.292	4.369	4.406

As seen in Table 3, the B3LYP functional gives an increase of the c lattice constant with increase of x for BCTO. This contradicts other results in this table, which show that a and c constants of the tetragonal structures shrink with increase of Sr (or Ca) concentration. Based on data from Table 3, the dependences c/a vs. x are plotted in Figure 1. Essentially different behaviour of these dependences for BSTO and BCTO solid solutions (the decrease for BSTO, but the rise for BCTO) attracts the attention. These trends are qualitatively reproduced using all three functionals. The decrease of c/a for BSTO is consistent with the fact that at large values of x BSTO exists in a cubic phase. Such behaviour of c/a ratio for BSTO coincides with existing

experimental data [12,33]. Detailed comparison of experimental and calculated (without taking into account configurational disorder) structural properties of BSTO solid solutions in tetragonal and cubic phases is presented in our paper [34]. In BCTO the situation is more complicated (tetragonal ratio grows, perhaps, with a saturation) and may be related to essential size mismatch between Ba and Ca atoms (off-center displacement of the smaller Ca ion in the Ba site) and the specific bond lengths of Ca ions in BCTO [11,12,16]. More detailed local structural analysis is necessary to clarify this problem and we plan to do this in a future paper. The compositional dependences of *c*/*a* for BSTO and BCTO shown in Figure 1 agree, at least, qualitatively, with the experimental data [12] (for BSTO — the fall of *c*/*a* ratio with increasing of dopant concentration, for BCTO — the rise with saturation and, perhaps, the fall afterwards). However, other experimental work [35] has shown an opposite trend in BCTO, i.e. a decrease in tetragonal ratio with increasing *x*, similar to that in BSTO.

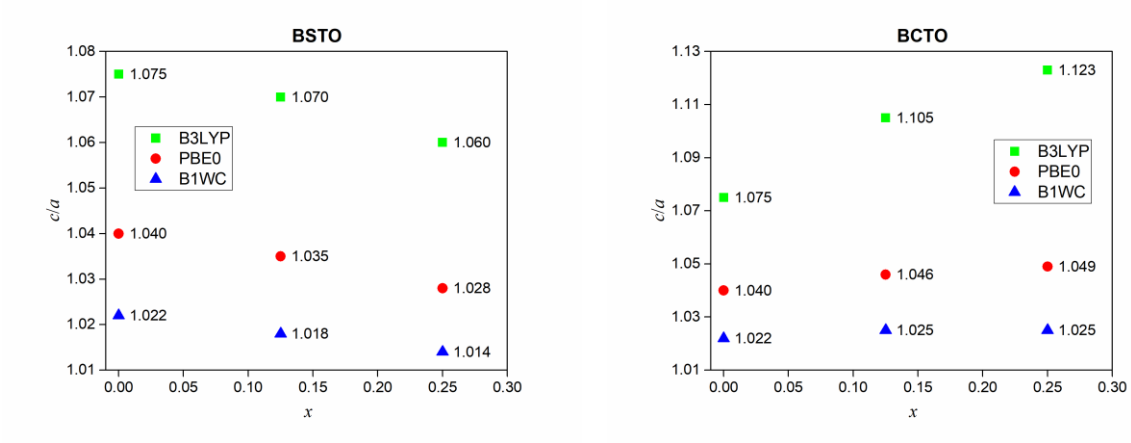

(a) (b)

Figure 1. Dependences of tetragonal ratio *c*/*a* vs. chemical composition *x* for BSTO (a) and BCTO (b), calculated by 3 functionals.

On the other hand, the trends in dependences of the unit cell volume of BSTO and BCTO vs. *x* (see Figure 2) are, at least, qualitatively identical — in the calculations, using all three functionals, volume decreases continuously with increasing dopant concentration. Such behaviour of unit cell volume in dependence on dopant concentration is logical — Ba atoms are replaced by smaller Sr atoms or far smaller Ca atoms. It is also reasonable to assume that this decrease should be larger for BCTO solid solution. Experimental data [12] indeed confirm this assumption. In our calculations, such trends are demonstrated only by data, obtained for the B1WC functional (volume of BCTO unit cell at *x*=0.25 is approximately 2.4% smaller than

of pure BTO). Moreover, the data, obtained by the B1WC functional, quantitatively are the closest to the experimental data [12].

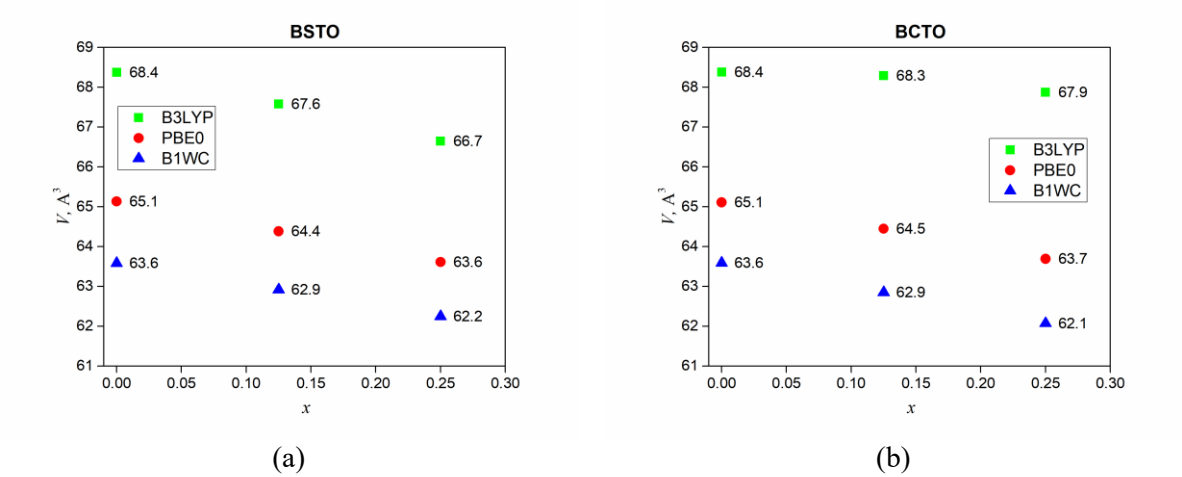

(a) (b)

Figure 2. Dependences of unit cell volume *V* vs. chemical composition *x* for BSTO (a) and BCTO (b), calculated by 3 functionals.

As was pointed out earlier [17], the experimental value of *c*/*a* for BTO in the tetragonal phase is 1.011. As one can see in Figure 1, the results of calculations using all functionals are overestimated for *x*=0. The B1WC functional demonstrates the best agreement, the worst — B3LYP. In our opinion, both PBE0 and B1WC functionals are suited well for the simulation of BSTO solid solution, but only B1WC (from 3 functionals which are used in this work) is preferable for BCTO computation. In turn, it is necessary to notice that the results in Table 3 are calculated with the XLGRID parameter and with increase of accuracy (the use of XXLGRID parameter) results change very little. On the other hand, computations of the electromechanical properties (especially of BCTO solid solution) are more sensitive to the accuracy of calculations; therefore, our further discussions are based on the computations with the XXLGRID parameter, performed for BSTO and BCTO solid solutions using the B1WC functional.

In the last part of the paper, we discuss and compare elastic and piezoelectric properties of BSTO and BCTO solid solutions for different chemical compositions. However, before this, let us consider in detail three tetragonal configurations of BCTO solid solution at the *x*=0.25 composition (we do not discuss here the four orthorhombic configurations). We report in Table 4 selected structural and electromechanical properties of these three configurations (a similar table providing information about all seven possible configurations for BSTO, is given in ref. [17]).

Table 4. Lattice constants and selected elastic and piezoelectric constants of the BCTO solid solution at the x=0.25 chemical composition, calculated using the B1WC functional for the tetragonal atomic configurations.

	(0.5, 0.5, 0.5)[a]	(0.5, 0.5, 0.0)[a]	(0.0, 0.0, 0.5)[a]	average[b]
		lattice constants, Å		
$a=b$	3.921	3.933	3.926	3.927
c	4.051	4.003	4.024	4.026
		elastic constants, GPa		
C_{11}	317.0	327.7	325.5	323.4
C_{12}	117.2	127.8	117.9	121.0
C_{13}	98.3	94.0	95.3	95.9
C_{33}	117.8	142.1	141.1	133.7
		direct piezoelectric constants, C/m^2		
e_{31}	0.842	0.934	0.928	0.901
e_{33}	4.762	6.128	5.168	5.353
		converse piezoelectric constants, pC/N = pm/V		
d_{31}	-11.586	-9.427	-8.140	-9.718
d_{33}	59.755	55.610	47.608	54.324

[a] Fractional coordinates in supercell of second Ca atom, which replaces of Ba atom. The first Ca atom is located at the origin of coordinates (0, 0, 0).
[b] Average value of parameter on 3 configurations.

Average values of lattice constants of BCTO solid solution at x=0.25 from Table 4 were used already in Table 3. Table 4 shows large differences in some parameters for the three configurations. For example, maximal difference for the elastic C_{33} constants is 21%, for the direct piezoelectric constants e_{33} — 29%, for the converse piezoelectric constants d_{31} — even 42% (cf. a value of 9% for d_{31} in the case of BSTO). These are rather big differences, therefore it is necessary to take into account configurational disorder in simulation of BCTO solid solutions.

Note the averaging problem of converse piezoelectric constants. As calculations of $\mathbb{d}$ tensor are based on the earlier calculated $\mathbb{C}$ and $\mathbb{e}$ tensors, it seems reasonable, that average values of converse piezoelectric constants have to be calculated using preliminary averaged elements of the elastic and direct piezoelectric tensors, while in Table 4 we average converse piezoelectric constants, obtained earlier for each tetragonal configuration. We calculated the converse piezoelectric tensor $\mathbb{d}$ directly as the product of $\mathbb{e}$ and $\mathbb{C}^{-1}$ tensors using the average values of elastic and direct piezoelectric constants from Table 4. The results of these calculations differ from those presented in Table 4 by less than 1.5%. This difference is considered as negligible, especially as we are interested in the analysis of trend of change of piezoelectric properties depending on the chemical composition.

Let us return now to BSTO and BCTO solid solutions. The elastic and piezoelectric constants of BSTO and BCTO at different dopant concentrations, obtained using the B1WC functional, are presented in Table 5 (simulation of BSTO by PBE0 functional was described in [17]).

Table 5. Some elastic and piezoelectric constants for BSTO and BCTO at different chemical composition *x*, calculated using the B1WC functional.

	BTO	BSTO				BCTO			
	x=0	*x*=0.125	%[a]	*x*=0.25	%	*x*=0.125	%	*x*=0.25	%
				Elastic constants (GPa)					
C_{11}	328	332	1%	337	3%	326	-1%	323	-2%
C_{12}	122	122	0%	122	0%	121	-1%	121	-1%
C_{13}	97	98	1%	100	3%	97	0%	96	-1%
C_{33}	157	165	5%	177	13%	141	-10%	134	-15%
				Direct piezoelectric constants (C/m^2)					
e_{31}	0.681	0.728	7%	0.798	17%	0.788	16%	0.901	32%
e_{33}	4.391	5.015	14%	5.848	33%	4.820	10%	5.353	22%
				Converse piezoelectric constants (pC/N=pm/V)					
d_{31}	-6.140	-6.730	10%	-7.197	17%	-7.990	30%	-9.718	58%
d_{33}	35.519	38.442	8%	41.130	16%	45.120	27%	54.324	53%

[a] Columns "%" are a change of constants at given *x* with regards to a pure BTO (*x*=0).

Table 5 reveals contrasting behaviour of the electromechanical properties of BSTO and BCTO solid solutions. The elastic properties of BSTO and BCTO demonstrate opposite trends (as well as the tetragonal ratios): while BSTO becomes mechanically harder when Ba atoms are substituted with Sr atoms (it was also predicted in [17]), the elastic constants of BCTO, in contrast, decrease. At the same time, the piezoelectric properties of BTO are improved in both BSTO and BCTO solid solutions with an increase of Sr or Ca concentration from 0 till 25%, i.e., qualitatively similar behaviour of piezoelectric properties as a function of chemical composition occurs for both solid solutions (as well as for dependences of unit cell volumes).

Let us look at the quantitative changes of electromechanical properties in more detail. The elements of BSTO and BCTO elastic tensors exhibit really opposite trends: changes of constants are similar, but with opposite signs. C_{33} constants demonstrate a maximal change: +13% for BSTO and -15% for BCTO at *x*=0.25. The direct piezoelectric constants show a gradual (and almost linear) rise, up to 20–30% at *x*=0.25 for both solid solutions. Thus, we predict a significant enhancement of the direct piezoelectric properties of BTO when replacing 25% of Ba atoms by Sr or Ca atoms. It is possible to note, that BSTO and BCTO "complement" each other: e_{33} constant grows by ~30% in BSTO and by ~20% in BCTO; at the same time, e_{31} constant grows by ~20% in BSTO and by ~30% in BCTO. The difference in behaviour of

converse piezoelectric properties of BSTO and BCTO is very interesting. Indeed, the absolute values of these constants grow in both solid solutions with increasing of dopant concentration, but the rise rate in BCTO is 3 times higher. In BCTO at x=0.25 these constants are increased more than by 50%. Thus, BCTO solid solution may be especially useful for improvement of converse piezoelectric constants. Such difference in converse piezoelectric properties of BSTO and BCTO is related, mainly, with different behaviour of the elastic constants of solid solutions. It is possible to prove this directly, using the above mentioned relation $\mathbb{d} = \mathbb{e}\,\mathbb{C}^{-1}$. The structure of tensors in this relation for the tetragonal system (6 independent constants for elastic tensor and 3 independent elements for piezoelectric tensors) is such that d_{31} and d_{33} constants depend only on the elements of elastic and direct piezoelectric tensors, presented in Table 5. Direct calculations show that C_{33}, as the least stable element of elastic tensor, defines the behaviour of converse piezoelectric constants.

Finally, we remind that, in computations, the elastic and piezoelectric constants could be theoretically presented as sums of the purely electronic ("clamped-ion") and nuclear relaxation components. We calculated in ref. [17] both these contributions for BTO and concluded that the origin of the piezoelectricity in BTO is mostly due to nuclear relaxation, whereas the electronic contribution is rather small. Now we have performed such calculations for both (BSTO and BCTO) solid solutions at all dopant concentrations. Our main conclusion is the same — nuclear relaxation contributes mainly to the piezoelectricity of solid solutions. However, it is interesting that in BCTO electronic contributions change only a little — for x=0.25 absolute values grow no more than by 5% in a comparison with pure BTO. In contrast, in BSTO the absolute values of "clamped-ion" components decrease considerably — by 13% for direct piezoelectric constants and by 17% for converse constants (at x=0.25). At the same time, the electronic component of all elastic constants in both solid solutions change very little (in the range of ±3% for x=0.25) and do not demonstrate excess variability at C_{33} constants.

Summing up, a few experimental studies could be mentioned in order to compare our theoretical trends of piezoelectric properties of BSTO and BCTO solid solutions with those obtained experimentally. Unfortunately, there are not enough experimental data on piezoelectric constants of solid solutions in the literature and they are partly contradictory. Thus, M.M. Kržmanc *et al.* reported 20 pm/V for d_{33} in BSTO (x=0.054) plates [33]. Authors [15] report the value of $d_{33} \sim 180$ pm/V for the BCTO single crystal in the range of $x = 0.1 – 0.25$. Wand with coauthors obtained converse piezoelectric constant $d_{33} \approx 150$ pm/V in BCTO ceramics at x=0.23 [36]. No doubt, more measurements of piezoelectric properties of

solid solutions are necessary. Piezoelectric properties depend on many parameters (size of crystal or ceramics, processing of sample, measurement conditions, etc.). Therefore, it would be better in the future to compare theoretical and experimental *trends* rather than numerical values of constants.

4. Conclusions

Based on advanced hybrid functionals of DFT and using supercell model, we performed *ab initio* simulations of tetragonal (room temperature) phases of $Ba_{(1-x)}Sr_xTiO_3$ and $Ba_{(1-x)}Ca_xTiO_3$ perovskite solid solutions and compared their structural and electromechanical properties at different chemical compositions x. We have shown that both PBE0 and B1WC hybrid functionals are well suited for a description of structural parameters and elastic and piezoelectric properties of BSTO solid solutions, while for BCTO simulations (these calculations are more sensitive to used functionals and accuracy) the B1WC functional is more preferable. We established that configurational disorder is important for BCTO simulations, while in BSTO this effect is rather small. It could be interesting in the future to analyse the effect of configurational disorder in BCTO by means of a thermodynamic approach [37]. BSTO and BCTO solid solutions reveal opposite behaviour of the tetragonal ratio c/a and elastic constants as the functions of chemical composition. On the other hand, both BSTO and BCTO reveal significantly enhanced piezoelectric properties (direct and converse) in comparison with pure BTO. Indeed, direct piezoelectric constants e_{33} and e_{31} grow by more than 30% at x=0.25 in BSTO and BCTO, respectively. Due to the decrease of elastic constants, BCTO may be especially useful for improvement of converse piezoelectric constants of BTO — at x=0.25 the absolute values of converse piezoelectric constants d_{31} and d_{33} increase by ~55% in BCTO, but only by 17% in BSTO.

Acknowledgments

This research was supported by the ERA-NET HarvEnPiez project. Many thanks to R. Dovesi, M.M. Kržmanc and D. Gryaznov for fruitful discussions.

References

[1] B. Jaffe, W.R. Cook, H. Jaffe, Piezoelectric ceramics, Academic Press, London, 1971.

[2] M.E. Lines, A.M. Glass, Principles and applications of ferroelectrics and related materials, Clarendon, Oxford, U.K., 1977.

[3] G.A. Smolenskii, V.A. Bokov, V.A. Isupov, N.N. Krainik, R.E. Pasynkov, A.I. Sokolov, N.K. Yushin, Ferroelectrics and related materials, Gordon and Breach, New York, 1984.

[4] C.R. Bowen, H.A. Kim, P.M. Weaver, S. Dunn, Piezoelectric and ferroelectric materials and structures for energy harvesting applications, Energy Environ. Sci. 7 (2014) 25−44, https://doi.org/10.1039/c3ee42454e.

[5] J. Rödel, W. Jo, K.T.P. Seifert, E-M. Anton, T. Granzow, D. Damjanovic, Perspective on the development of lead-free piezoceramics, J. Am. Ceram. Soc. 92 (2009) 1153–1177, https://doi.org/10.1111/j.1551-2916.2009.03061.x.

[6] M. Acosta, N. Novak, V. Rojas, S. Patel, R. Vaish, J. Koruza, G.A. Rossetti Jr., J. Rödel, $BaTiO_3$-based piezoelectrics: Fundamentals, current status, and perspectives, Appl. Phys. Rev. 4 (2017) 041305, https://doi.org/10.1063/1.4990046.

[7] J. Gao, D. Xue, W. Liu, C. Zhou, X. Ren, Recent progress on $BaTiO_3$-based piezoelectric ceramics for actuator applications, Actuators 6 (2017) 24, https://doi.org/10.3390/act6030024.

[8] V.V. Lemanov, A.V. Sotnikov, E.P. Smirnova, M. Weihnacht, R. Kunze, Perovskite $CaTiO_3$ as an incipient ferroelectric, Solid State Communications 110 (1999) 611–614, https://doi.org/10.1016/S0038-1098(99)00153-2.

[9] R. Ali, M. Yashima, Space group and crystal structure of the perovskite $CaTiO_3$ from 296 to 1720K, Journal of Solid State Chemistry 178 (2005) 2867–2872, https://doi.org/10.1016/j.jssc.2005.06.027.

[10] M. Yashima, R. Ali, Structural phase transition and octahedral tilting in the calcium titanate perovskite $CaTiO_3$, Solid State Ionics 180 (2009) 120–126, https://doi.org/10.1016/j.ssi.2008.11.019.

[11] D. Fu, M. Itoh, S. Koshihara, T. Kosugi, S. Tsuneyuki, Anomalous phase diagram of ferroelectric $(Ba,Ca)TiO_3$ single crystals with giant electromechanical response, Phys. Rev. Lett. 100 (2008) 227601, https://doi.org/10.1103/PhysRevLett.100.227601.

[12] I. Levin, V. Krayzman, J.C. Woicik, Local-structure origins of the sustained Curie temperature in (Ba,Ca)TiO_3 ferroelectrics, Appl. Phys. Lett. 102 (2013) 162906, https://doi.org/10.1063/1.4802996.

[13] V.V. Lemanov, E.P. Smirnova, P.P. Syrnikov, E.A. Tarakanov, Phase transitions and glasslike behavior in $Sr_{1-x}Ba_xTiO_3$, Phys. Rev. B 54 (1996) 3151–3157, https://doi.org/10.1103/PhysRevB.54.3151.

[14] S.W. Kim, H.I. Choi, M.H. Lee, J.S. Park, D.J. Kim, D. Do, M.H. Kim, T.K. Song, W.J. Kim, Electrical properties and phase of $BaTiO_3$–$SrTiO_3$ solid solution, Ceram. Int. 39 (2013) S487−S490, https://doi.org/10.1016/j.ceramint.2012.10.119.

[15] D. Fu, M. Itoh, S. Koshihara, Crystal growth and piezoelectricity of $BaTiO_3$–$CaTiO_3$ solid solution, Appl. Phys. Lett. 93 (2008) 012904, https://doi.org/10.1063/1.2956400.

[16] J.A. Dawson, D.C. Sinclair, J.H. Harding, C.L. Freeman, A-site strain and displacement in $Ba_{1-x}Ca_xTiO_3$ and $Ba_{1-x}Sr_xTiO_3$ and the consequences for the curie temperature, Chemistry of Materials 26 (2014) 6104−6112, https://doi.org/10.1021/cm502158n.

[17] L.L. Rusevich, G. Zvejnieks, A. Erba, R. Dovesi, E.A. Kotomin, Electromechanical properties of $Ba_{(1-x)}Sr_xTiO_3$ perovskite solid solutions from first-principles calculations, J. Phys. Chem. A 121 (2017) 9409–9414, https://doi.org/10.1021/acs.jpca.7b08473.

[18] R. Dovesi *et al*., CRYSTAL14: A program for the *ab initio* investigation of crystalline solids, Int. J. Quantum Chem. 114 (2014) 1287−1317, https://doi.org/10.1002/qua.24658.

[19] R. Dovesi *et al*., CRYSTAL14 user's manual, University of Torino, Torino, 2014.

[20] S. Piskunov, E. Heifets, R.I. Eglitis, G. Borstel, Bulk properties and electronic structure of $SrTiO_3$, $BaTiO_3$, $PbTiO_3$ perovskites: An *ab initio* HF/DFT study, Comput. Mater. Sci. 29 (2004) 165–178, https://doi.org/10.1016/j.commatsci.2003.08.036.

[21] T. Bredow, K. Jug, R.A. Evarestov, Electronic and magnetic structure of $ScMnO_3$, Phys. Stat. Sol. (b) 243 (2006) R10−R12, https://doi.org/10.1002/pssb.200541403.

[22] L. Valenzano, F.J. Torres, K. Doll, F. Pascale, C.M. Zicovich-Wilson, R. Dovesi, *Ab initio* study of the vibrational spectrum and related properties of crystalline compounds; the case of $CaCO_3$ calcite, Z. Phys. Chem. 220 (2006) 893–912, https://doi.org/10.1524/zpch.2006.220.7.893.

[23] O. Madelung, U. Rössler, M. Schulz (Eds.), Ternary compounds, organic semiconductors, in: Landolt-Börnstein — Group III Condensed Matter, vol. 41E, Springer, Berlin, 2000.

[24] L. Cao, E. Sozontov, J. Zegenhagen, Cubic to tetragonal phase transition of $SrTiO_3$ under epitaxial stress: An X-ray backscattering study, Phys. Stat. Sol. (a) 181 (2000) 387−404, https://doi.org/10.1002/1521-396X(200010)181:2<387::AID-PSSA387>3.0.CO;2-5.

[25] M.L. Moreira, E.C. Paris, G.S. do Nascimento, V.M. Longo, J.R. Sambrano, V.R. Mastelaro, M.I.B. Bernardi, J. Andres, J.A. Varela, E. Longo, Structural and optical properties of $CaTiO_3$ perovskite-based materials obtained by microwave-assisted hydrothermal synthesis: An experimental and theoretical insight, Acta Mater. 57 (2009) 5174−5185, https://doi.org/10.1016/j.actamat.2009.07.019.

[26] N.L. Ross, R.J. Angel, Compression of $CaTiO_3$ and $CaGeO_3$ perovskites, Am. Mineral. 84 (1999) 277−281, https://doi.org/10.2138/am-1999-0309.

[27] G.J. Fischer, Z. Wang, S. Karato, Elasticity of $CaTiO_3$, $SrTiO_3$ and $BaTiO_3$ perovskites up to 3.0 GPa: The effect of crystallographic structure, Phys. Chem. Miner. 20 (1993) 97−103, https://doi.org/10.1007/BF00207202.

[28] A. Linz Jr., K. Herrington, Electrical and optical properties of synthetic calcium titanate crystal, J. Chem. Phys. 28 (1958) 824−825, https://doi.org/10.1063/1.1744278.

[29] A. Boudali, A. Abada, M.D. Khodja, B. Amrani, K. Amara, F.D. Khodja, A. Elias, Calculation of structural, elastic, electronic, and thermal properties of orthorhombic $CaTiO_3$, Phys. B 405 (2010) 3879−3884, https://doi.org/10.1016/j.physb.2010.06.020.

[30] K.S. Knight, Structural and thermoelastic properties of $CaTiO_3$ perovskite between 7K and 400K, J. Alloys Compd. 509 (2011) 6337−6345, https://doi.org/10.1016/j.jallcom.2011.03.014.

[31] T. Bak, J. Nowotny, C.C. Sorrel, M.F. Zhou, Electronic and ionic conductivity in $CaTiO_3$, Ionics 10 (2004) 334−342, https://doi.org/10.1007/BF02377992.

[32] R.I. Eglitis, A.I. Popov, Systematic trends in (001) surface *ab initio* calculations of ABO_3 perovskites, J. Saudi Chem. Soc. 22 (2018) 459−468, https://doi.org/10.1016/j.jscs.2017.05.011.

[33] M.M. Kržmanc, H. Uršič, A. Meden, R.C. Korošec, D. Suvorov, $Ba_{1-x}Sr_xTiO_3$ plates: Synthesis through topochemical conversion, piezoelectric and ferroelectric characteristics, Ceram. Int. 44 (2018) 21406−21414, https://doi.org/10.1016/j.ceramint.2018.08.198.

[34] L.L. Rusevich, G. Zvejnieks, E.A. Kotomin, M. Maček Kržmanc, A. Meden, Š. Kunej, I.D. Vlaicu, Theoretical and experimental study of (Ba,Sr)TiO_3 perovskite solid

solutions and $BaTiO_3/SrTiO_3$ heterostructures, J. Phys. Chem. C 123 (2019) 2031−2036, https://doi.org/10.1021/acs.jpcc.8b09750.

[35] R. Varatharajan, R. Jayavel, C. Subramanian, Growth and characterization of ferroelectric $Ba_{1-x}Ca_xTiO_3$ single crystals, Ferroelectrics 215 (1998) 169−180, https://doi.org/10.1080/00150199808229560.

[36] X. Wang, H. Yamada, C.-N. Xu, Large electrostriction near the solubility limit in $BaTiO_3$–$CaTiO_3$ ceramics, Appl. Phys. Lett. 86 (2005) 022905, https://doi.org/10.1063/1.1850598.

[37] D. Fuks, S. Dorfman, S. Piskunov, E.A. Kotomin, *Ab initio* thermodynamics of $Ba_cSr_{(1-c)}TiO_3$ solid solutions, Phys. Rev. B: Condens. Matter Mater. Phys. 71 (2005) 014111, https://doi.org/10.1103/PhysRevB.71.014111.

Institute of Solid State Physics, University of Latvia as the Center of Excellence has received funding from the European Union's Horizon 2020 Framework Programme H2020-WIDESPREAD-01-2016-2017-TeamingPhase2 under grant agreement No. 739508, project CAMART²